International Conference on Space Optics—ICSO 2022

Dubrovnik, Croatia

3–7 October 2022

Edited by Kyriaki Minoglou, Nikos Karafolas, and Bruno Cugny,

Calibration of Einstein Probe FXT – QM and FM at the PANTER X-ray test facility

Calibration of Einstein Probe FXT – QM and FM
at the PANTER X-ray test facility

Surangkhana Rukdee[a], Peter Friedrich[a], Vadim Burwitz[a], Gisela Hartner[a], Thomas Müller[a],
Thomas Schmidt[a], Andreas Langmeier[a], and Konrad Dennerl[a]

[a]MPI for Extraterrestrial Physics, Giessenbachstrasse 1, 85748 Garching, Germany

ABSTRACT

The Follow-up telescope (FXT) is one of the instruments on board for the Einstein Probe mission, a dedicated mission to the study of the time-domain high-energy astrophysics due to launch end of 2023. The full calibration tests were carried out at the PANTER X-ray test facility, of the Max-Planck Institute for extraterrestrial Physics in Germany, to validate the performance of the fully flight-compatible optics, both the Qualification Model (QM) and the Flight Model (FM). The eROSITA Wolter-I-type telescope, consisting of 54 X-ray mirror shells was characterised in terms of the angular resolution and effective area. The effective areas were measured using the "Glücksrad" that allows quasi-parallel beam measurements to simulate the in-orbit scenario. The TRoPIC and PIXI detectors were used to take the exposures. A silicon drift detector mounted sidelong in the tube, out of the optic's field of view, was installed to monitor the X-ray beam simultaneously. The QM telescope experienced a slight degradation of the half energy width (HEW) at Al-K energy (1.49 keV) during the thermal cycle test while the FM satisfied the requirements. Both modules satisfied the effective area requirement at this standard energy. In this work, we discuss the full calibration tests at different energies for the Einstein Probe FXT – QM and FM. The measured HEW, effective area, vignetting, and final focal length at PANTER will be summarized.

Keywords: Wolter Telescope, X-ray, Calibration, Instrumentation

1. INTRODUCTION

The Einstein Probe (EP)[1] is a dedicated mission for time-domain high-energy astrophysics led the Chinese Academy of Sciences (CAS) due to launch in 2023. The primary goals of the mission are to discover high-energy transients, to monitor variable objects and to search for X-ray sources associated with gravitational-wave events. The instruments on board consists of 1) the Wide-Field X-ray Telescope (WXT)[2] providing a 3,600 square degrees field of view within the energy range of 0.5-4 keV[3] and 2) the Follow-Up X-ray Telescope (FXT)[4] for the energy range 0.3-10 keV high resolution follow-up observations.

The Einstein Probe follow-up telescope[4] (FXT) is the European contribution, funded by the European Space Agency (ESA), accomplished by Media Lario S.r.l., Italy, and the Max Planck Institute for Extraterrestrial Physics (MPE). The FXT is an eROSITA-like Wolter-I-type telescope,[5] consisting of 54 gold-coated nickel X-ray mirror shells[6] mounted inside a case with an interface to the telescope structure, where the mirror shells are glued into a spoke wheel ('spider'). After an acceptance test with X-rays, the X-ray baffle (XRB) was precisely aligned and mounted to the mirror module. Thereafter, it is referred to as a mirror assembly (MA). The main goal of the final X-ray test and calibration is to evaluate the optic performance in terms of angular resolution (PSF images) and effective area as a function of energy of the MA. The test requirements are described in Table 1.

Further author information: (Send correspondence to S.R.)
S.R.: E-mail: suri@mpe.mpg.de

Table 1. Requirements for orbit and derived requirements for PANTER X-ray test

	Orbit	Derived for PANTER
HEW Al-K (1.49 keV)	$< 22''$	$< 22''$
Eff. Area Al-K	$> 350 cm^2$	$> 348.2 cm^2$
Eff. Area Cu-K	$> 20 cm^2$	$> 18.7 cm^2$
Micro-roughness	$< 0.5 nm$	Scattering Cu-K $< 15.7\%$
Focal length	$1600 \pm 2mm$	$1600 \pm 2mm$

2. SETUP & ALIGNMENT

The Einstein Probe FXT FM mirror module was delivered directly to the PANTER X-ray test facility from Media Lario. The mirror passed its the acceptance test at PANTER. After the assembly of the baffle[7] and all the environmental tests carried out at MPE in Garching, the optic was installed inside the chamber for the final calibration tests. Only the multi-target X-ray source in full illumination will be used in this campaign (available X-ray lines from 0.18 to 9.88 keV). This section describes setup and alignment metrology inside the PANTER chamber. During the test, the TRoPIC CCD detector was mainly used to take the exposures. A silicon drift detector (SDD) mounted sidelong in the tube, out of the optic's field of view, was available to monitor the X-ray beam simultaneously.

2.1 Layout inside Chamber

The layout of the PANTER chamber is displayed in Figure 1. The vacuum chamber is 12 m long and has a diameter of 3.5 m. This can be separated into two parts: 1) the source tube (left), 2) a big chamber (right) where the optic is installed. At the source end, a 6.5 mm diameter aperture was mounted 1.538 m from the X-ray source, to create a beam of approx. 510 mm diameter at the location of the optic, ensuring full beam coverage of the optic. The target source in full illumination is used in this campaign. The multi-target X-ray source can generate a bremsstrahlungs continuum plus characteristic X-ray lines in the range 0.18 to 9.88 keV. At a distance of ~35 m from the X-ray source, a silicon drift detector (SDD) is installed to monitor the beam stability during the campaign.
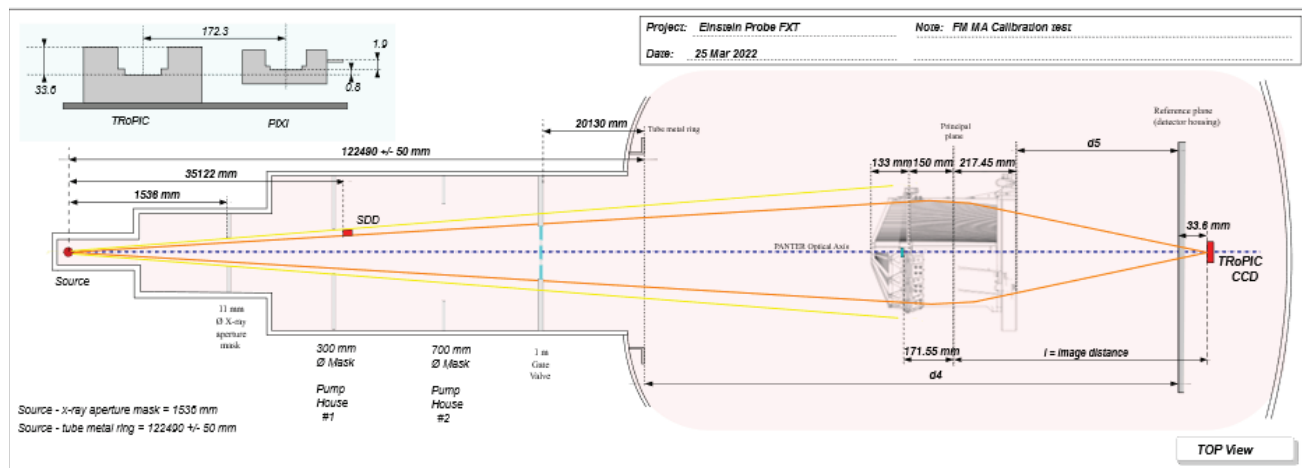

Figure 1. The overall layout inside the chamber, with key distances and angles labelled, to be measured during the setup of the campaign.

Inside the big chamber, a "Glücksrad" shown in Figure 3 is used to illuminate sectors of the MA with a "quasi" parallel beam, a beam generated from a point source at a far distance away from optic. The Glücksrad

consists of two independently rotatable masks on the same rotation axis which allow the illumination of selectable sectors of the MA aperture. Each wheel is equipped with 4 alignment pinholes. The FXT optic, is placed on the base plate of the manipulator. The manipulator can translate to left-right or so called Wald-Pantolsky direction. There are two rotation angles in pitch and yaw, necessary for the tip-tilt and rotation characterization of the optic. In addition, there is also a detector manipulator that can also translate up-down, Wald-Pantolsky and along the optical axis (Quelle-Küche) – see Figure 2.
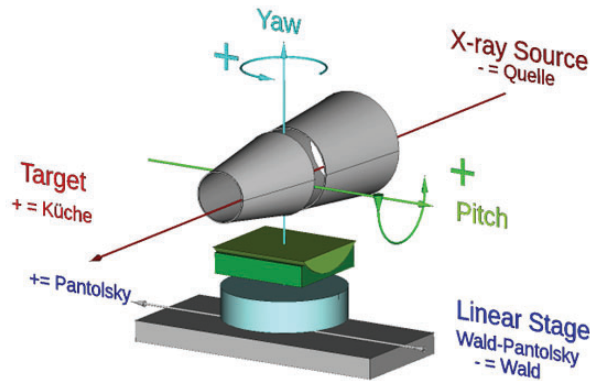

Figure 2. The coordinate system of the optics when mounted at PANTER

2.2 Alignment of Optic

2.2.1 Pre-alignment

To make the alignment of the X-ray image on the detector easier, a pre-alignment using a visible laser – see also Figure 3, is carried out before the chamber is closed and put under vacuum. The X-ray source is removed from the source tube. The laser is mounted in the same position as the X-ray source and the beam travels down the same beamline to the optics. The optic is positioned on the laser optical axis. The covered centre of the optic was used to auto-collimate the alignment laser beam. This alignment position of the optic was the 'laser alignment' position.
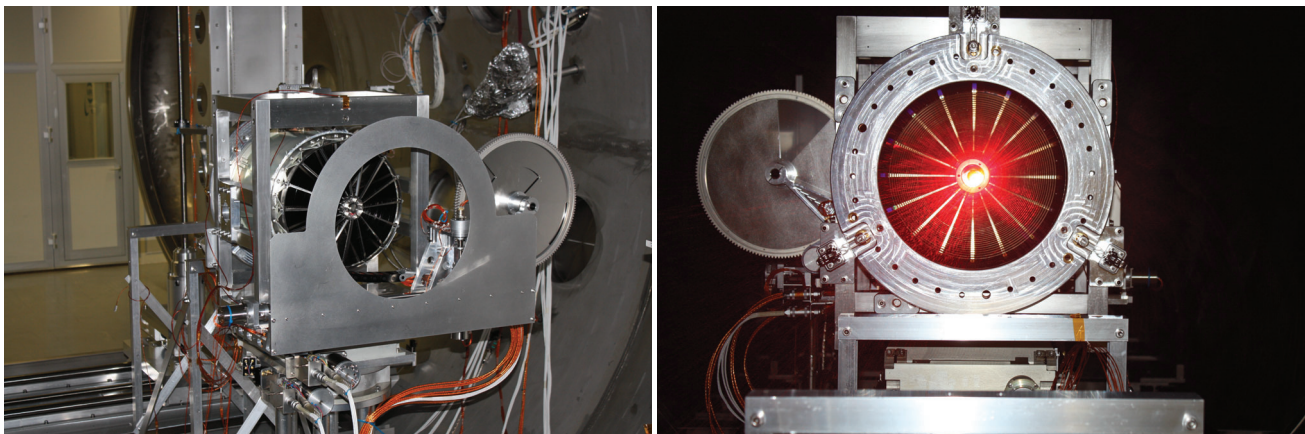

Figure 3. The FXT installed inside the PANTER chamber. (Left) the front side of the mirror assembly looking from the source. The Glücksrad is installed in the front of the mirror assembly.(Right) The back side of the mirror assembly during the laser alignment.

2.2.2 Burkert Test

The Burkert test[8] was carried out in full illumination in the double reflection position for a coarse alignment. The aim of the test was to align the optic in pitch and yaw using single reflections from the full MA. The optic was aligned iteratively, with alterations in pitch and yaw angle after the initial positions were observed. Although the Burkert test was performed under full illumination, only the single reflections from the innermost shell – Shell 54 – were used for alignment. A high beam intensity allows quick visualisation of the single reflection structures.
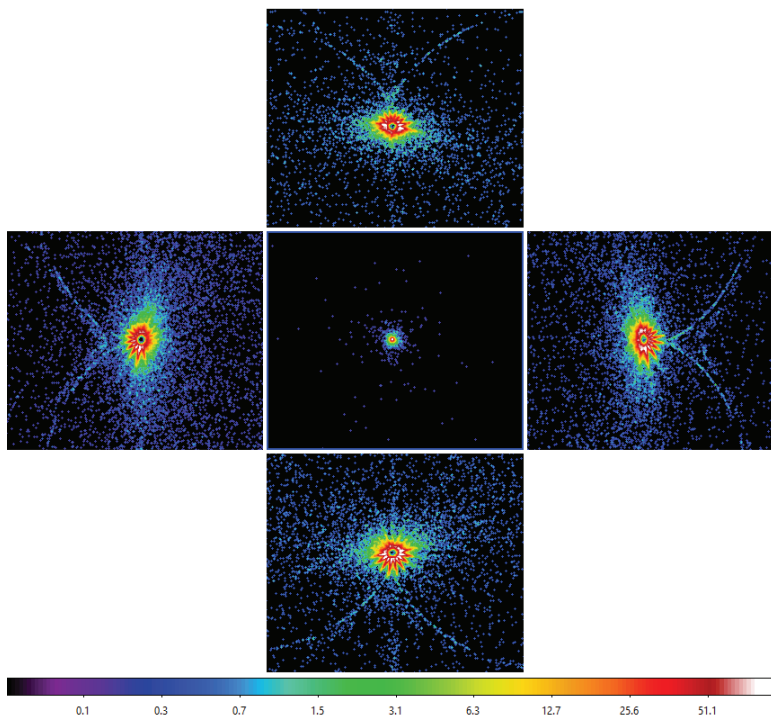

Figure 4. The Burkert test result at Al-K. Clockwise from top with angles relative to laser alignment: positive pitch (+19.0 arcmin), negative yaw (-20.1 arcmin), negative pitch (-16.0 arcmin), positive yaw (+15.5 arcmin). The central image is the resulting on-axis PSF, in preliminary best focus.

During the Burkert test, the higher-than-usual heating voltages led to a 'hole' at the centre of the double reflected image as shown in Figure 4. This is caused by the pile-up effect on the TRoPIC detector. For the Burkert test this 'hole' is acceptable, as only the geometry of the single reflection "arcs" with respect to the PSF centre is required.

2.2.3 Egger-Menz Test

Once the Burkert test had preliminarily determined the best pitch and yaw angles, the Egger-Menz test[8] was carried out to confirm these positions. This test determines the final best pitch and yaw angles, the on-axis position of the MA. Contrary to the Burkert test, the Egger-Menz test is sensitive to the full mirror system and not only for one shell. This test requires a pitch scan and a yaw scan of the optic, where at each pitch/yaw position an intra-focal image is taken. From each position the azimuthal intensity distribution of the image is determined. For a perfectly aligned mirror the intensity distribution is homogeneous, but for an off-axis angle the intensity distribution becomes elliptical.[8] Using the phase and amplitude of the second Fourier component of each image, the amount of off-axis angle can be quantified. The detector was moved 60 mm intra-focal relative to the laser alignment position for these measurements. The Egger-Menz pitch scan was completed first and followed by the yaw scan. Using steps of 3 arcmin, the scans were made around the best Burkert pitch and yaw position from -15 arcmin to +15 arcmin, with 600 seconds integration time per position.

3. MEASUREMENT METHODS

3.1 Focus search

In preparation of the detailed 6x6 pixel scans at different local distances, a rough focus search around the laser alignment nominal image distance position, with PIXI was conducted, in order to get a good starting point for the precise focus search with TRoPIC.

With the TRoPIC detector, the focus search is the scan along the optical axis at a series of intra- and extra-focal positions around the nominal in-focus position (the laser alignment position) to determine the minimum HEW of the MA, at the energy Al-K (1.49 keV). At each position a 6×6 pixel scan (step width 12.5 μm, corresponding to 10 manipulator steps) with an exposure of 60 seconds was performed with TRoPIC.

3.2 Effective Area

The effective area measurement is done using the Glücksrad for the on-axis quasi-parallel illumination. The Glücksrad is a mechanical device to be used in the PANTER X-ray test facility for the effective area measurements of eROSITA-like mirror modules – such as EP-FXT – with an almost parallel beam. It consists of two independently rotatable masks on the same rotation axis which allow the illumination of selectable sectors of the mirror module aperture as shown in Figure 5. It has a high precision angular positioning system and well defined zero-positions for each mask. The masks are mounted into a frame which is placed in front of the mirror module (on the same stage). The Glücksrad can be operated remotely in the PANTER vacuum chamber.
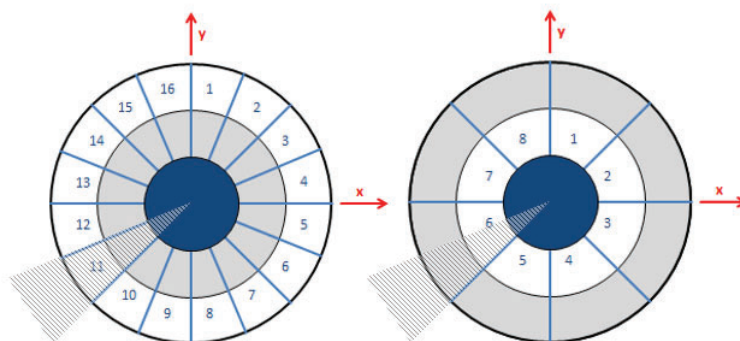

Figure 5. Sectors illuminated in almost parallel beam by the "Glücksrad" one after the other; left: outer sectors for shells 1 to 18 with 22.5 ° azimuthal width, right: inner sectors for shells 19 to 54 with 45 ° azimuthal width; the support structure of the "Glücksrad" blocks the outer sector 11 fully and half of the inner sector 6 (shaded area).

The measurements were carried out at five energies in on-axis and intra-focal position: Al-K (1.49 keV), Ag-L(2.98, 3.15, 3.35, 3.52 keV), Ti-K(4.51, 4.93 keV), Fe-K(6.4, 7.06 keV), Cu-Kα (8.04 keV), and at the continuum energy ranges lEbc (0.8-4.0 keV), mEbc (2.35-8.0 keV). At each position an exposure was taken for approx. 5,000 counts. Before and after each measurement set a flat field (FF) exposure was taken, for approx. 1,500 counts. The flat field exposures serve as a reference for the X-ray beam, as the collecting area of detector is well defined; the region of interest of TRoPIC is 3.516 cm^2. During a flat field measurement, the optic and Glücksrad are removed from the X-ray beam, and TRoPIC remains in the on-axis, intra-focal position. The use of two flat field exposures accounts for possible beam variations over the measurement period. The effective area values in this report are corrected using the flat field exposures. Fifteen outer 22.5 ° sectors (shells 1 to 18) and eight inner 45° sectors (shells 19 to 54) were separately measured with TRoPIC. For each sector, the MA was turned in pitch/yaw such that the centre of the sector is perpendicular to the line-of-sight to the X-ray source. This way the sector is illuminated with an almost parallel beam.

The effective area A_{eff} was calculated using Equation 1, where C_{optic} is the count rate from the optic, C_{FF} is the flat field count rate, A_{det} is the collecting area of the detector (3.516 cm^2), and G is the geometrical correction for the divergent X-ray beam.

$$A_{\text{eff}} = \frac{C_{\text{optic}}}{C_{\text{FF}}} \times A_{\text{det}} \times G \tag{1}$$

The geometrical correction, G, is calculated using Equation 2, where the distance between the source and the optic is $d_{\text{source-optic}}$. The effective area is measured at the image distance d_{image}. The value for G for this campaign is 0.9734.

$$G = \left(\frac{d_{\text{source-optic}}}{d_{\text{source-optic}} + d_{\text{image}}} \right)^2 \tag{2}$$

The 1σ relative statistical error is calculated for each exposure, using the number of counts in the region of interest on the detector. This error is propagated through the above calculation to give a 1σ error on the effective area value of each exposure.

3.3 Deep PSF Exposures

The deep PSF images were made using the same pixel scan method described in Section 6.4.2 The detector was moved in Wald-Pantolsky and Up-Down in a 12×12 grid with a pitch of 6.25 μm scanning the in-focus on-axis PSF. over a full TRoPIC pixel – 75 × 75 μm^2. To avoid edge effects caused by TRoPIC's electronical signal processing components (one CAMEX for 128 pixel columns each) the image centre was positioned close to the "Zauberpixel" (pixel coordinates 104, 128), a sweet spot for the measurement due to the detector chips arrangement. The measurement is done at 3 photon energies: C-K (0.28 keV), Al-K (1.49 keV) and Cu-Kα (8.04 keV). Each exposure (at each of the 12×12 positions) was 150 seconds in length. The count rate was adjusted to approx. 0.54 counts/s over the full relevant spectral band, i.e. line + bremsstrahlung in an area of 3×3 pixels on the detector in order to avoid pile-up signals that would falsify the PSF result. This type of measurement allows a deep detailed PSF measurement to be made, as scanning over the pixel avoids pattern type bias. This is necessary because the PSF is so small that the photons encircled in the "HEW circle" during the analysis are mainly detected in one pixel.

3.4 Focal Plane Mapping

The focal plane mapping (FPM) was done primarily to obtain a vignetting curve, but it also delivers some information on the off-axis PSF. The method uses several off-axis positions over a 1 degree by 1 degree field-of-view (FOV), which corresponds to the detector size used for FXT. The time consumption was kept relatively low, as each position gets only 80 seconds exposure time, while the source flux was maximized. The consequent high count rates cause pile-up, which however can be taken into account by the analysis software that adds up also all counts in the multiples of the used characteristic line. The FOV is covered by using two grids of data points, shown in Figure 6:

1) The wider grid consists of 8 by 8 positions that range from -28' to +28' in steps of +8', both in yaw and pitch.

2) The smaller grid consists of 5 by 5 positions that range from -6' to +6' in steps of +3', both in yaw and pitch.

Both grids are complementary since the wider one covers the entire course of the vignetting curve, while the smaller one reveals its central part. Both grids are centered on the measured optical axis (see 2.2), but the analysis of the FPM allows to correct this position. The detector position during FPM is fixed, since the mirror tilting in yaw and pitch lets the images always appear at (almost) the same location.

Before and after each of the scans (at least one) flat field measurements were done to monitor the X-ray beam. All FPM measurements were done at -0.4 mm intra-focal. The Glücksrad was put out of the beam in park position. The FPM was done at 5 energies: Al-K, Ag-L, Ti-K, Fe-K and Cu-K. Note that for Fe-K and Cu-K a different gain setting of the TRoPIC detector was used (gain EC) in order to extend the measurable energy band such that all relevant pile-up peaks could be found.
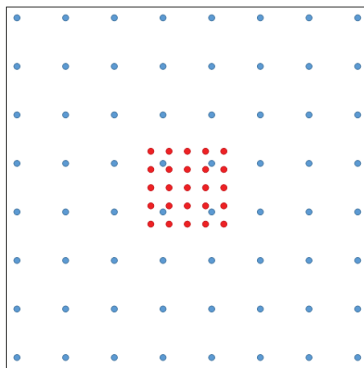
Figure 6. The two grids for focal plan mapping in a 60 arcmin × 60 arcmin square.

3.5 Focal Length Measurement

After the final set of X-ray measurements, the detector was moved into the best focus position, on axis. The chamber was vented, and the focal length measurement was performed. The mechanical-optical gauge[8] was inserted in the MM's blocking shell and positioned to measure the distance between the MM's reference mirror (in the centre of the spider wheel) and the detector CCD chip. The detector was moved incrementally towards the gauge until it was detected by the gauge sensor, ensuring no damage to the CCD chip. The range of the sensor is up to 2500 μm. Reference measurements were done before and after, using a standard that had been calibrated with a coordinate measuring machine to an accuracy of 5 μm. Due to the uncertainty of the exact position of the principal plane of the optic, the focal length can be determined with an accuracy of 0.5 mm only. However, more important is the knowledge of the distance between the reference mirror and the the surface of the CCD chip, which can be determined with an accuracy of about 40 μm. This distance will be used during the assembly of the FXT, when optic and detector are mounted into the telescope structure.

4. RESULTS

The measurement results are presented in the this section. Effective area, Focal plane mapping and deep exposures are presented separately for both, QM and FM calibration campaigns.
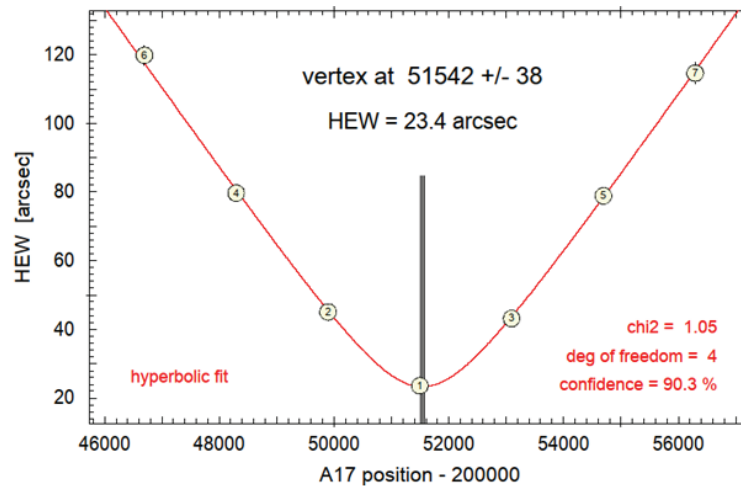
4.1 QM

4.1.1 Focus Search

The measurement result of the focus search is obtained from moving the detector around the rough best focus position in the range of ±6mm along the optical axis. PSF analysis combines the 6x6 pixel scan for each position. The resulting focus curve (HEW vs focus position 'A17') is then fitted with a hyperbola fit as shown in Figure 7 where the minimum HEW of 23.4 arcsec corresponds to the best focus position.

4.1.2 Deep PSF Exposures

This measurement allows a deep detailed PSF measurement to be made, as scanning over the pixel avoids pattern type bias. This is necessary because the PSF is so small that the photons encircled in the "HEW circle" during the analysis are mainly detected in one pixel. The results summary of the on-axis deep PSF measurement is in Table 2.

Sets of images were taken with PIXI at intra- and extra- focal position to observe the defects and deformation in Figure 8. This is caused by the either vibration or thermal test, on the mirror shells. The intra-focal images were taken at -80 mm and the extra-focal images were taken at +80 mm from the best focus position.

Figure 7. The compilation results of the focus search and the hyperbola fit to determine the best focus position, the smallest PSF (minimum of HEW), for the QM at Al-K.

Table 2. Summary of the Deep PSF measurement at different energies, for the QM.

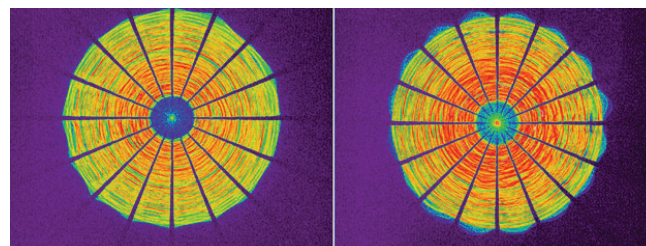| Energy	HEW [arcsec]	W90 [arcsec]	Scattering Fraction
Al-K	23.8 ± 0.3	117.3	0.057
Cu-K	25.7 ± 0.4	323.8	0.203
C-K	23.8 ± 0.4	100.6	0.040

Figure 8. The compilation of images of the deep PSF of the QM at Al-K with PIXI intra- (left), and extra-focal (right).

4.1.3 Effective Area

The effective area measurements with the Glücksrad were carried out at -50 mm intra-focal position and illuminating all 8 inner- and 16 outer sectors one after the other in an almost parallel beam. The measurement at Al-K, Ag-L, Ti-K energies were carried out for both inner and outer sectors while at Fe-K and Cu-K were done only for the inner sectors. The compilation of images at each energy is displayed in Figure 9 with the summary of the effective area at inner sectors, outer sectors and the full optic is in Table 3. The summary on the low energy band continuum measurements is shown in Figure 10. The measured data points at different energies were plotted over the continuum measurement at lEbc.
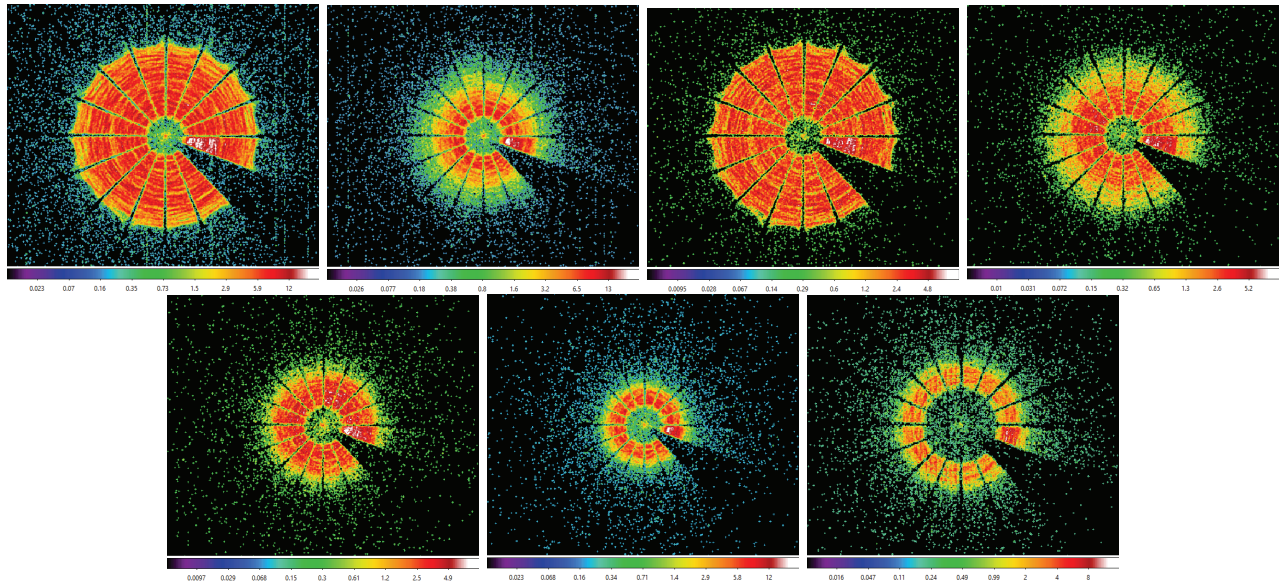
Figure 9. Compilation of intra-focal images for different sectors of the QM MA selected by different positions of the Glücksrad at different energies: (Top row) lEbc, mEbc, Al-K, Ag-L (Bottom row) Ti-K, Fe-K, Cu-K respectively, for the qualification model. Sector 11 is fully obscured by the support arm of the Glücksrad.
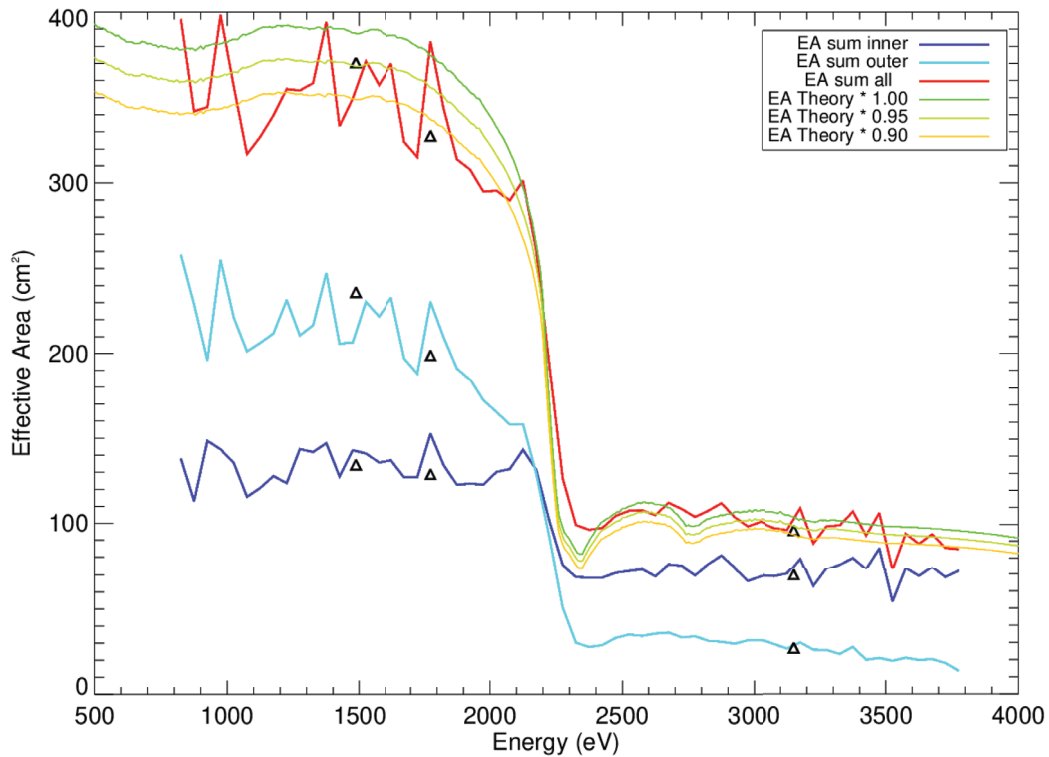

Figure 10. The effective area measurements of the QM MA overlaid with the theoretical model. The summary of effective area at low energy band continuum at different sectors are shown with different color: dark blue for inner sectors, light blue for the outer sectors and red for the total mirror. The small triangles are the measured data points for the energies Al-K, W-M and Ag-L.

Table 3. Summary of the effective area at different energies, for the QM

Energy	Inner Sectors	Outer Sectors	Total (full optic)
Al-K	134.42 ± 2.28	236.08 ± 2.93	370.50 ± 3.72
Ag-L	69.58 ± 0.54	26.81 ± 0.24	96.39 ± 0.60
Ti-K	62.54 ± 0.82	3.86 ± 0.08	66.40 ± 0.82
Fe-K	33.52 ± 0.21	-	-
Cu-K	18.18 ± 0.33	-	-

4.1.4 Focal Plane Mapping and Vignetting

The results from the two overlapping grids, as described in 3.4, are shown in Figure 11. The FPM measurements, all in 0.4 mm intra-focal position and with boosted count rate, were performed for 5 photon energies: Al-K (1.49 keV), Ag-L (2.98 keV), Ti-K (4.51 keV), Fe-K (6.40 keV), Cu-Kα (8.04 keV).
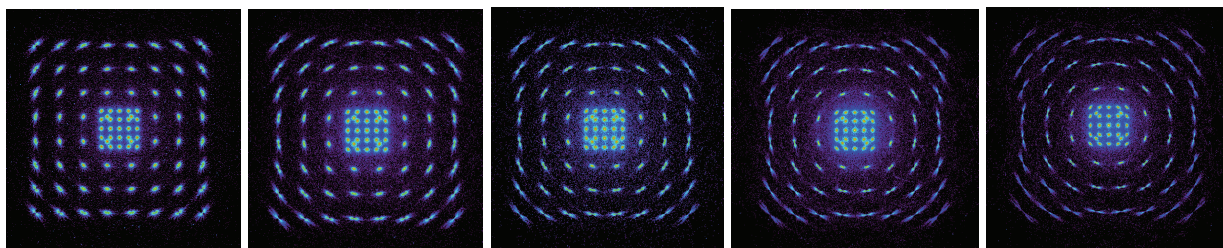

Figure 11. Composed focal plane mapping at different energies (left to right) Al-K, Ag-L, Ti-K, Fe-K, Cu-K respectively for the QM.

The vignetting curves for these 5 energies are derived from the FPM by analysing the count rates in each of the 89 off-axis positions, resulting in count rates as a function of off-axis angle. Finally, a fitting function is applied with the on-axis position as a free parameter. Figure. 12 shows the normalised vignetting: As expected, the vignetting becomes steeper with increasing energy. Due to the large number of positions the curves are well defined, without being harmed by a few outliers.
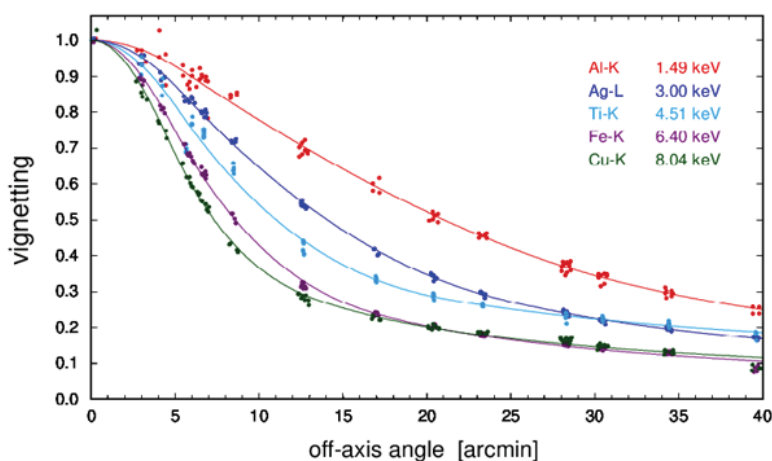

Figure 12. Vignetting curves for all five energies: Al-K, Ag-L, Ti-K, Fe-K, and Cu-K in comparison for the QM.

4.1.5 Focal Length Measurement

The measured distance between the MA reference mirror and the CCD chip (in focus) is 1792.870 mm $\pm$ 0.021 mm. Applying several corrections, the target value of this distance in the orbit case is calculated as 1773.182 mm $\pm$ 0.040 mm. The focal length is derived with less accuracy because of uncertainties about the exact position of the MA principal plane. The derived focal length of the QM MM is 1601.63 mm $\pm$ 0.5 mm.

4.2 FM

4.2.1 Focus Search

The PSF analysis, for the focus search, combines the 6x6 pixel scan for each focus position in the range of $\pm$6mm. The resulting focus curve (HEW vs focus position 'A17') is then fitted with a hyperbola fit as shown in Figure 13 where the minimum HEW of 21.9 arcsec corresponds to the best focus position.

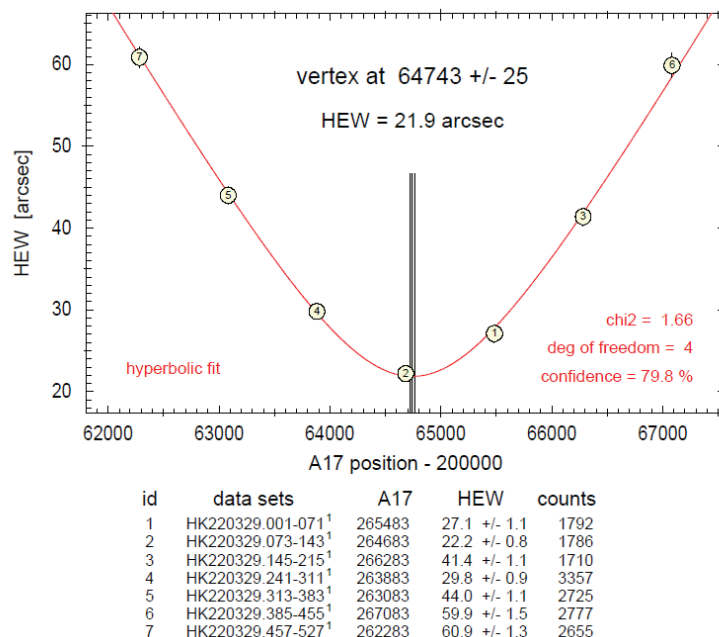| id	data sets	A17	HEW	counts
1	HK220329.001-071[1]	265483	27.1 +/- 1.1	1792
2	HK220329.073-143[1]	264683	22.2 +/- 0.8	1786
3	HK220329.145-215[1]	266283	41.4 +/- 1.1	1710
4	HK220329.241-311[1]	263883	29.8 +/- 0.9	3357
5	HK220329.313-383[1]	263083	44.0 +/- 1.1	2725
6	HK220329.385-455[1]	267083	59.9 +/- 1.5	2777
7	HK220329.457-527[1]	262283	60.9 +/- 1.3	2655

Figure 13. The compilation results of the focus search and the hyperbola fit to determine the best focus position, the smallest PSF (minimum of HEW), for the FM at Al-K.

4.2.2 Deep PSF Exposures

This measurement allows a deep detailed PSF measurement to be made, as scanning over the pixel avoids pattern type bias. The photons encircled in the "HEW circle" during the analysis are mainly detected in one pixel as shown in Figure 14. The results summary of the on-axis deep PSF measurement is in Table 4.

Table 4. Summary of the Deep PSF measurement at different energies, for the FM

Energy	HEW [arcsec]	W90 [arcsec]	Scattering Fraction
C-K	21.9 ± 0.3	93.6	0.027
Al-K	21.9 ± 0.3	107.5	0.049
Cu-K	25.3 ± 0.4	350.2	0.177

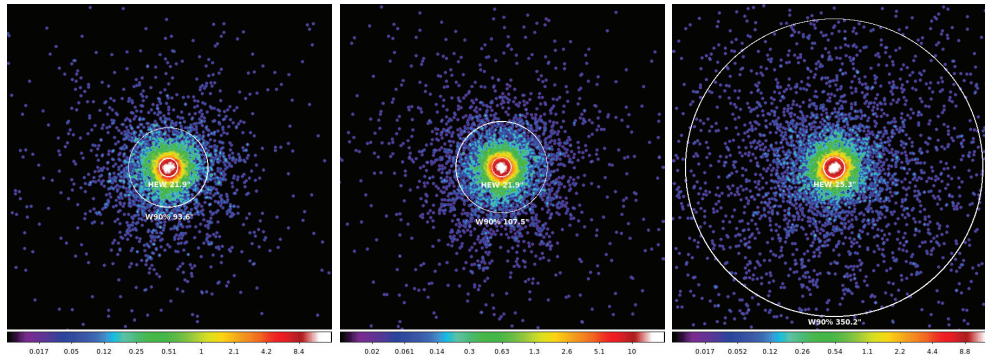Figure 14. Image of the zoomed region ($256\times 256\ \mu m^2$ or 32.6×32.6 arcsec^2) around the PSF centre, with the HEW marked as white circles, at different energies: (left to right) C-K, Al-K, Cu-K

The intra- and extra- focal images were taken with PIXI to observe the defects and deformation, caused by the either vibration or thermal test, on the mirror shells. The intra-focal images were taken at -80 mm and the extra-focal images were taken at +80 mm from the best focus position.
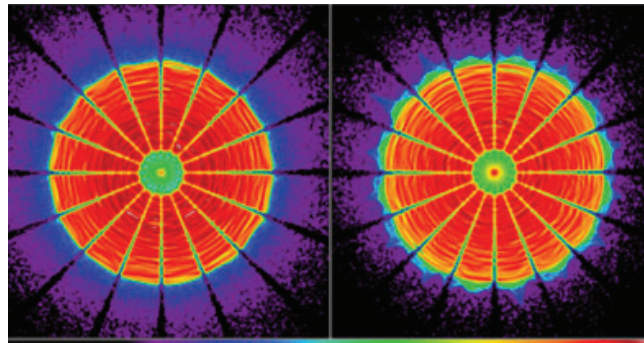

Figure 15. The compilation of images of the deep PSF at Al-K with PIXI intra- (left), and extra-focal (right) for the FM.

4.2.3 Effective Area

The effective area measurements with the Glücksrad were performed at -50 mm intra-focal position and illuminating all 8 inner- and 16 outer sectors one after the other in an almost parallel beam. At Fe-K and Cu-K, only the inner sectors were used, because the outer shells do not reflect at these energies. The compilation of images for the FM Effective area measurement is in Figure 16. In addition, effective area measurements were done with continuum spectra from about 0.8 keV to 8 keV and summarised in Table 5. The low- and mid- Energy band continuum are plotted in Figure 17.

Table 5. Summary of the effective area at different energies for the FM

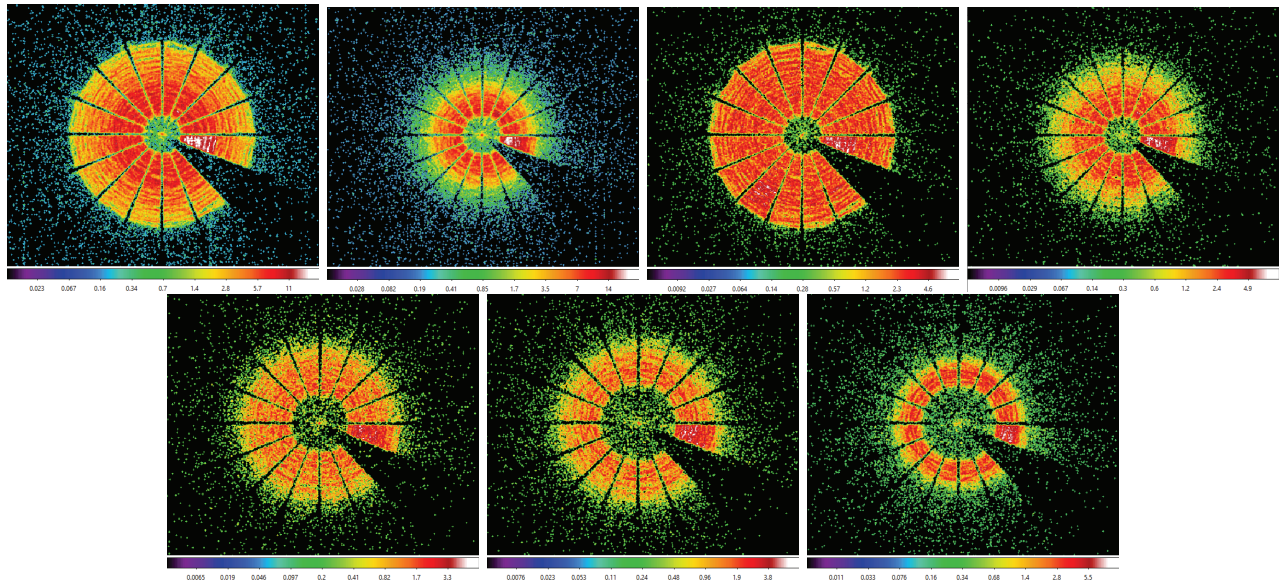| Energy	Inner Sectors	Outer Sectors	Total (full optic)
Al-K	137.16 ± 2.21	223.54 ± 2.63	360.70 ± 3.43
Ag-L	68.13 ± 1.08	26.48 ± 0.36	94.61 ± 1.14
Ti-K	63.28 ± 0.81	3.80 ± 0.09	67.08 ± 0.82
Fe-K	33.66 ± 0.30	-	-
Cu-K	17.92 ± 0.13	-	-

Figure 16. Compilation of intra-focal images for different sectors of the FM MA selected by different positions of the Glücksrad at different energies: (Top row) lEbc, mEbc, Al-K, Ag-L (Bottom row) Ti-K, Fe-K, Cu-K respectively, for the flight model. Sector 11 is fully obscured by the support arm of the Glücksrad.
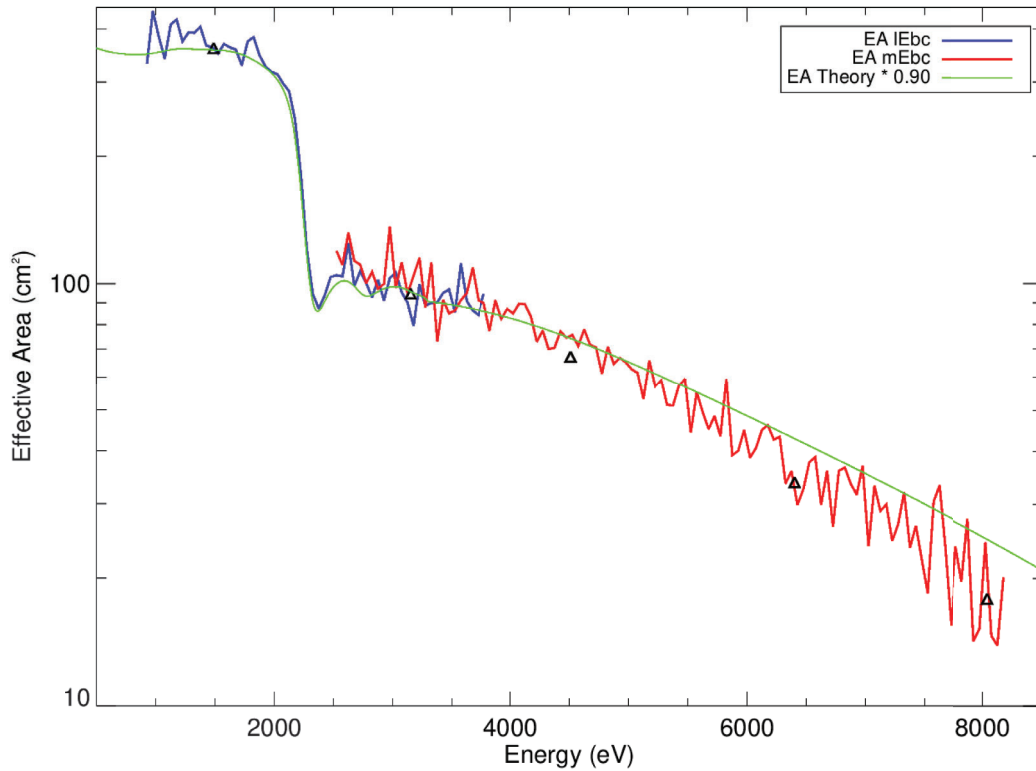

Figure 17. The effective area measurements for the FM MA overlaid with the theoretical model. The summary of effective area at low and medium energy band continuum are shown with different color: green is 90% of the theoretical value, dark blue for the lEbc, and red for the mEbc, for the full optic. The small triangles are the measured data points for the energies Al-K, Ti-K, Fe-K and Cu-K.

4.2.4 Focal Plane Mapping and Vignetting

Focal plane mappings were carried out at 5 different energies in the same way as for the QM: Al-K, Ag-L, Ti-K, Fe-K, Cu-K. The analysis is identical to the one applied for the QM calibration and is described in 4.1.4. The resulting focal plane maps and the derived vignetting curves for the FM are shown in Figure 18 and 19, respectively.
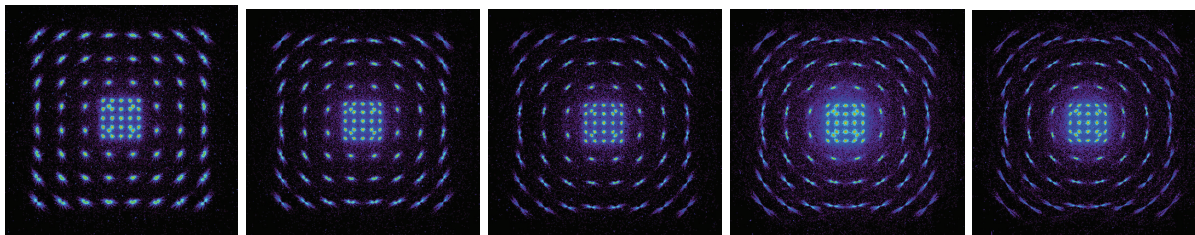

Figure 18. Composed focal plane mapping at different energies (left to right) Al-K, Ag-L, Ti-K, Fe-K Cu-K for the FM
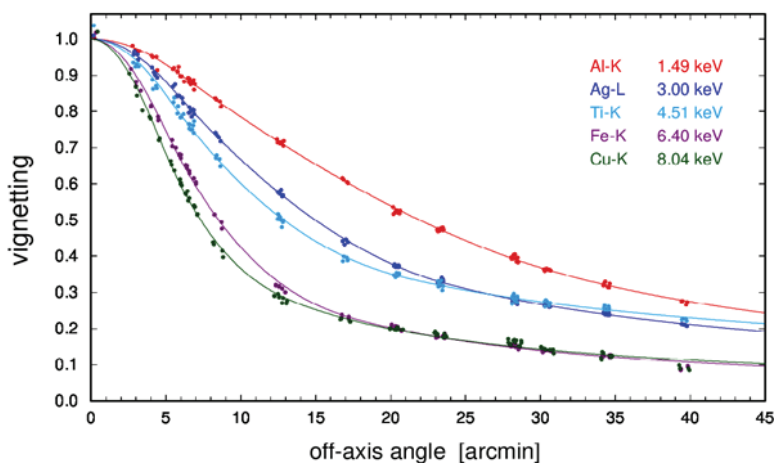

Figure 19. Vignetting curves for all five energies: Al-K, Ag-L, Ti-K, Fe-K, and Cu-K in comparison for the FM.

4.2.5 Focal Length Measurement

The measured distance between the MA reference mirror and the CCD chip (1.5 mm extra-focal) is 1794.786 mm $\pm$ 0.021 mm. After corrections, the target value of this distance in the orbit case is calculated as 1773.520 mm $\pm$ 0.040 mm. This distance is important for flight units to later adjust of camera and mirror assemblies in the telescope structure. The focal length is derived with less accuracy because of uncertainties about the exact position of the MA principal plane. The derived focal length of the FM MA is 1601.97 mm $\pm$ 0.5 mm.

5. DISCUSSION & CONCLUSION

In this work, we report the full calibration tests at different energies for the Einstein Probe FXT – QM and FM at the PANTER X-ray test facility. The X-ray calibration test was done after the thermal cycling and vibration tests. They reflect the measured optical performance of the QM and FM Mirror Assembly under laboratory conditions prior to delivery. Beyond the optical performance listed in the Table 6, the calibration includes many more measurements at different photon energies, which are reported in detail in the previous sections. The effective areas were measured using the "Glücksrad", a device that allows measurements with a quasi-parallel beam that simulates almost the situation in orbit, where X-ray sources are at an "infinite" distance.

Table 6. Summary of the calibration measurements for the FXT QM and FM

	Orbit	PANTER	QM	FM
HEW Al-K (1.49 keV)	< 22"	< 22"	23.8 ± 0.3"	21.9 ± 0.3"
HEW Cu-K (8.04 keV)	-	-	25.7 ± 0.4"	25.3 ± 0.4"
Eff. Area Al-K	$> 350 cm^2$	$> 348.2 cm^2$	$370.50 \pm 3.72 cm^2$	$360.70 \pm 3.43 cm^2$
Eff. Area Cu-K	$> 20 cm^2$	$> 18.7 cm^2$	$18.18 \pm 0.33 cm^2$	$17.92 \pm 0.13 cm^2$
Micro-roughness	$< 0.5 nm$	Scattering Cu-K $< 15.7\%$	20.3%	17.7%
Focal length	$1600 \pm 2 mm$	$1600 \pm 2 mm$	$1601.63 \pm 0.5 mm$	$1601.97 \pm 0.5 mm$

For the QM, the optical performance in terms of HEW degraded slightly during the TC test, while there was no performance change after vibration as seen at the STM MA.[6] A reduction of the on-axis effective area at high energies was observed after the mounting of the X-ray baffle; this is due to the tight nesting of the inner mirror and baffle shells, where a slight misalignment can cause partial shading. For the FM, the HEW, effective area measurement at Al-K and focal length measurement meet the requirements, although the effective area at the Cu-K energy has 1% less than the expected value. The micro-roughness was measured to be 2% higher than the requirement. However, the measured optical performance in the laboratory is not identical to that what is expected during operation in orbit. There are a number of possible error contributions that finally reduce the optical performance. The required measurement results are summarized in Table 6.

In conclusion, the QM telescope experienced a slight degradation of the half energy width (HEW) at Al-K energy (1.49 keV) during the thermal cycle test while the FM satisfied the requirements. Both modules satisfied the effective area requirement at the standard energy as well as the focal length.

ACKNOWLEDGMENTS

REFERENCES

[1] Yuan, W., Zhang, C., Feng, H., Zhang, S. N., Ling, Z. X., Zhao, D., Deng, J., Qiu, Y., Osborne, J. P., O'Brien, P., Willingale, R., Lapington, J., Fraser, G. W., and the Einstein Probe team, "Einstein Probe - a small mission to monitor and explore the dynamic X-ray Universe," *arXiv e-prints* , arXiv:1506.07735 (June 2015).

[2] Yuan, W., Zhang, C., Ling, Z., Zhao, D., Wang, W., Chen, Y., Lu, F., Zhang, S.-N., and Cui, W., "Einstein Probe: a lobster-eye telescope for monitoring the x-ray sky," in [*Space Telescopes and Instrumentation 2018: Ultraviolet to Gamma Ray*], den Herder, J.-W. A., Nikzad, S., and Nakazawa, K., eds., *Society of Photo-Optical Instrumentation Engineers (SPIE) Conference Series* **10699**, 1069925 (July 2018).

[3] Feldman, C., O'Brien, P., Willingale, R., Zhang, C., Ling, Z., Yuan, W., Jia, Z., Jin, G., Li, L., Xu, Z., Zhang, Z., Lerman, H., Hutchinson, I., McHugh, M., and Lodge, A., "Testing of the WXT optics at the University of Leicester," in [*Society of Photo-Optical Instrumentation Engineers (SPIE) Conference Series*], *Society of Photo-Optical Instrumentation Engineers (SPIE) Conference Series* **11444**, 114447R (Dec. 2020).

[4] Chen, Y., Cui, W., Han, D., Wang, J., Yang, Y., Wang, Y., Li, W., Ma, J., Xu, Y., Lu, F., Chen, H., Tang, Q., Yuan, W., Friedrich, P., Meidinger, N., Keil, I., Burwitz, V., Eder, J., Hartmann, K., Nandra, K., Keereman, A., Santovincenzo, A., Vernani, D., Bianucci, G., Valsecchi, G., Wang, B., Wang, L., Wang, D., Li, D., Sheng, L., Qiang, P., Shi, R., Chao, X., Song, Z., Zhang, Z., Huo, J., Wang, H., Cong, M., Yang, X., Hou, D., Zhao, X., Zhao, Z., Chen, T., Li, M., Zhang, T., Luo, L., Xu, J., Li, G., Zhang, Q., Bi, X., Zhu, Y., Yu, N., Chen, C., Lv, Z., Lu, B., and Zhang, J., "Status of the follow-up x-ray telescope onboard the Einstein Probe satellite," in [*Society of Photo-Optical Instrumentation Engineers (SPIE) Conference Series*], *Society of Photo-Optical Instrumentation Engineers (SPIE) Conference Series* **11444**, 114445B (Dec. 2020).

[5] Predehl, P., Andritschke, R., Arefiev, V., Babyshkin, V., Batanov, O., Becker, W., Böhringer, H., Bogomolov, A., Boller, T., Borm, K., Bornemann, W., Bräuninger, H., Brüggen, M., Brunner, H., Brusa, M., Bulbul, E., Buntov, M., Burwitz, V., Burkert, W., Clerc, N., Churazov, E., Coutinho, D., Dauser, T., Dennerl, K., Doroshenko, V., Eder, J., Emberger, V., Eraerds, T., Finoguenov, A., Freyberg, M., Friedrich, P., Friedrich, S., Fürmetz, M., Georgakakis, A., Gilfanov, M., Granato, S., Grossberger, C., Gueguen, A., Gureev, P., Haberl, F., Hälker, O., Hartner, G., Hasinger, G., Huber, H., Ji, L., Kienlin, A. v., Kink, W., Korotkov, F., Kreykenbohm, I., Lamer, G., Lomakin, I., Lapshov, I., Liu, T., Maitra, C., Meidinger, N., Menz, B., Merloni, A., Mernik, T., Mican, B., Mohr, J., Müller, S., Nandra, K., Nazarov, V., Pacaud, F., Pavlinsky, M., Perinati, E., Pfeffermann, E., Pietschner, D., Ramos-Ceja, M. E., Rau, A., Reiffers, J., Reiprich, T. H., Robrade, J., Salvato, M., Sanders, J., Santangelo, A., Sasaki, M., Scheuerle, H., Schmid, C., Schmitt, J., Schwope, A., Shirshakov, A., Steinmetz, M., Stewart, I., Strüder, L., Sunyaev, R., Tenzer, C., Tiedemann, L., Trümper, J., Voron, V., Weber, P., Wilms, J., and Yaroshenko, V., "The eROSITA X-ray telescope on SRG," *A&A* **647**, A1 (Mar. 2021).

[6] Bradshaw, M., Burwitz, V., Friedrich, P., Hartner, G., Langmeier, A., Valsecchi, G., Vernani, D., and Chen, Y., "X-ray testing of the Einstein Probe follow-up x-ray telescope STM at MPE's PANTER facility," in [*Society of Photo-Optical Instrumentation Engineers (SPIE) Conference Series*], *Society of Photo-Optical Instrumentation Engineers (SPIE) Conference Series* **11444**, 1144457 (Dec. 2020).

[7] Friedrich, P., Rohé, C., Gaida, R., Hartwig, J., Soller, F., Bräuninger, H., Budau, B., Burkert, W., Burwitz, V., Eder, J., Hartner, G., Menz, B., and Predehl, P., "The eROSITA x-ray baffle," in [*Space Telescopes and Instrumentation 2014: Ultraviolet to Gamma Ray*], Takahashi, T., den Herder, J.-W. A., and Bautz, M., eds., *Society of Photo-Optical Instrumentation Engineers (SPIE) Conference Series* **9144**, 91444R (July 2014).

[8] Menz, B., Bräuninger, H., Burkert, W., Burwitz, V., Friedrich, P., and Hartner, G., "Alignment of eROSITA like mirrors at the PANTER x-ray test facility," in [*Optics for EUV, X-Ray, and Gamma-Ray Astronomy VI*], O'Dell, S. L. and Pareschi, G., eds., *Society of Photo-Optical Instrumentation Engineers (SPIE) Conference Series* **8861**, 88611I (Sept. 2013).